JOURNAL OF ENVIRONMENTAL SCIENCES 90 (2020) 375–384

Available online at www.sciencedirect.com

ScienceDirect

www.elsevier.com/locate/jes

JES JOURNAL OF ENVIRONMENTAL SCIENCES

www.jesc.ac.cn

Degradation of organic contaminants through the activation of oxygen using zero valent copper coupled with sodium tripolyphosphate under neutral conditions

Chengwu Zhang [1,2,3], *Lishuang Xuan* [1,2,3], *Jingyi Zhang* [1,2,3], *Fang Yuan* [1,2,3], *Xianglong Kong* [1,2,3], *Chuanyu Qin* [1,2,3,*]

[1] *Key Laboratory of Groundwater Resources and Environment, Ministry of Education, Jilin University, Changchun 130021, China*

[2] *Jilin Provincial Key Laboratory of Water Resources and Environment, Jilin University, Changchun 130021, China*

[3] *National and Local Joint Engineering Laboratory for Petrochemical Contaminated Site Control and Remediation Technology, Jilin University, Changchun 130021, China*

ARTICLE INFO

Article history:
Received 21 November 2019
Received in revised form
1 January 2020
Accepted 1 January 2020
Available online 13 January 2020

Keywords:
Sodium tripolyphosphate
Zero valent copper corrosion
Oxygen activation
pH control

ABSTRACT

In this study, sodium tripolyphosphate (STPP) was used to promote the removal of organic pollutants in a zero-valent copper (ZVC)/O_2 system under neutral conditions for the first time. 20 mg/L p-nitrophenol (PNP) can be completely decomposed within 120 min in the ZVC/O_2/STPP system. The PNP degradation process followed pseudo-first-order kinetics and the degradation rate of PNP gradually increased upon the decreasing ZVC particle size. The optimal pH of the reaction system was 5.0. Our mechanism investigation showed that Cu^+ generated by ZVC corrosion was the main reducing agent for the activation of O_2 to produce ROS. ·OH was identified as the only ROS formed during the degradation of PNP and its production pathway was the double-electron activation of O_2 ($O_2 \rightarrow H_2O_2 \rightarrow$ ·OH). In this process, STPP did not only promote the release of Cu^+ through its complexation, but also promoted the production of ·OH by reducing the redox potential of Cu^{2+}/Cu^+. In addition, we could initiate and terminate the reaction by controlling the pH. At pH < 8.1, ZVC/O_2/STPP could continuously degrade organic pollutants; at pH > 8.1, the reaction was terminated. STPP was recycled to continuously promote the corrosion of ZVC and O_2 activation as long as the pH was <8.1. This study provided a new and efficient way for O_2 activation and organic contaminants removal.

* *Corresponding author.*
E-mail address: qincyu@jlu.edu.cn (C. Qin).

https://doi.org/10.1016/j.jes.2020.01.001

Introduction

Advanced oxidation processes (AOPs) involving the generation of reactive oxygen species (ROS), such as hydroxyl radicals (·OH), are regarded as one of the most promising techniques for the degradation of organic pollutants (Cinar et al., 2017; Lee et al., 2007; Matzek and Carter, 2016; Yan et al., 2015; Zhao et al., 2014). The traditional Fenton reaction generates ·OH by reacting Fe^{2+} with H_2O_2 under acidic conditions. However, the use of H_2O_2 in the system has the disadvantages of poor stability, low utilization efficiency, and substantial environmental impact (Joseph et al., 2009; Saritha et al., 2007). Oxygen is a green, economic and readily available oxidant. In recent years, researchers have confirmed that metal elements, including iron and aluminum, can activate oxygen to produce ·OH (Bokare and Wonyong, 2009; Lin et al., 2014; Liu et al., 2011; Michael et al., 2011; Noradoun and I Francis, 2005; Welch et al., 2002). For example, Sedlak and coworkers (Keenan and Sedlak, 2008) found that EDTA was effectively degraded by a ZVI/O_2 system at pH 3.5 and reported the mechanism for ·OH production in the system in detail. Putschew and coworkers reached a similar conclusion. Similar to ZVI, zero-valent aluminum (ZVAl)/O_2 was also able to remove organic pollutants such as 2,4-dichlorophenol under acidic conditions (Lin et al., 2014). In addition to the above two metals, the activation of oxygen by Cu^+ has also been reported (Feng et al., 2017; Lee et al., 2016; Zhou et al., 2018). It can not only activate molecular oxygen to generate H_2O_2, but induce the decomposition of as-formed H_2O_2 to produce ·OH (Deng et al., 2019). It is well established that ·OH is produced upon the reaction of Cu^+ and O_2, but there is still a debate in regard the mechanism and pathway for the generation of ·OH in this system. Some researchers believe that the mechanism of ·OH production is the single-electron activation of O_2 ($O_2 \rightarrow O_2\cdot^- \rightarrow H_2O_2 \rightarrow \cdot OH$) (Xiu et al., 2012; Zhou et al., 2017). Specifically, Cu^+ activates O_2 to generate superoxide radicals ($O_2\cdot^-$) (Eq. (1)), and H_2O_2 and ·OH are then sequentially produced (Eqs. (2) and (3)). However, the other researchers believe that the production of ·OH is through the double-electron activation of O_2 ($O_2 \rightarrow H_2O_2 \rightarrow \cdot OH$) (Eqs. (3) and (4)) (Dong et al., 2014; Zhang et al., 2017). Therefore, it is necessary to further study the mechanism of ROS production in the Cu^+/O_2 reaction system.

$$Cu^+ + O_2 \rightarrow Cu^{2+} + O_2\cdot^- \quad (1)$$

$$Cu^+ + O_2\cdot^- + 2H^+ \rightarrow Cu^{2+} + H_2O_2 \quad (2)$$

$$Cu^+ + H_2O_2 \rightarrow Cu^{2+} + \cdot OH + OH^- \quad (3)$$

$$2Cu^+ + O_2 + 2H^+ \rightarrow 2Cu^{2+} + H_2O_2 \quad (4)$$

In addition, because Cu^+ cannot be present under ambient conditions (Moffett and Zika, 1987), how to continuously generate a sufficient amount of Cu^+ is also an urgent problem to be solved. At present, there are two main methods, one is to reduce Cu^{2+} to Cu^+ using a suitable reducing agent (Lee et al., 2016; Zhou et al., 2016). For example, Zhou et al. used ascorbic acid to reduce Cu^{2+} to produce Cu^+, and subsequently produced ·OH through the reaction of Cu^+ and O_2. The other method is to produce Cu^+ via the corrosive dissolution of zero valent copper (ZVC) (Dong et al., 2014). For instance, Wen et al. reported that diethyl phthalate (DEP) was completely oxidized in ZVC/O_2 after 120 min at an initial pH of 2.5. Because the former method has the disadvantage of short duration time and great difficulty to control the reaction rate, the ZVC/O_2 system is considered to have a better application prospect. However, since ZVC is difficult to corrode under neutral conditions (Lin et al., 2005; Huang et al., 2012), the system can only be used to degrade organic pollutants under acidic conditions. To the best of our knowledge, there is no report on the degradation of organic pollutants using the ZVC/O_2 system under neutral conditions. In the field of corrosion protection engineering, researchers have found that ligands, such as EDTA and sodium oxalate, can effectively promote the corrosion of ZVC (Tamura et al., 2001). Therefore, we speculated whether the ZVC/O_2 system can degrade organic pollutants under neutral conditions upon the addition of a suitable ligand.

In this study, p-nitrophenol (PNP) was used as the target contaminant. The effect of different ligands on the degradation efficiency of PNP in the ZVC/O_2 system was evaluated. According to the experimental results, STPP, a commonly used polyphosphate ligand, was selected to improve the oxidation efficiency of the ZVC/O_2 system. A series of experiments were carried out to reveal the mechanism for ROS generation and PNP degradation, and further explore the role of STPP in the reaction. Finally, we explored the influence of variables including the initial pH and STPP dosage on the reaction.

1. Materials and methods

1.1. Materials and reagents

ZVC powder with different particle size (particle size: 100 nm, 1 μm, 5 μm and 44 μm, purity: >99.9%) and catalase from bovine liver (BR, 2094 μg/mg) were purchased from Aladdin Reagent Co., Ltd. (Shanghai, China). Coumarin-3-carboxylic acid and bathocuproine were purchased from Sigma-Aldrich (Shanghai, China). Sodium tripolyphosphate (STPP, $Na_5P_3O_{10}$), ethylenediamine tetraacetic acid disodium salt (EDTA, $C_{10}H_{14}N_2Na_2O_8$, 99%), sodium oxalate ($C_2Na_2O_4$, 99%), 2,9-dimethyl-1,10-phenant-hroline (DMP, $C_{14}H_{12}N_2$, 98%), p-nitrophenol (PNP, $H_6H_5NO_3$, 99%), potassium iodide (KI, 99%), starch (99%), tert-butanol (TBA, $C_6H_{10}O$, 99%) and cuprous chloride (CuCl, 99%) were purchased from the Tianjin Guangfu Fine Chemical Research Institute (China). Ethanol (CH_3CH_2OH, 99.9%) was purchased from Beijing Chemical Works (China). All chemical reagents used in this study were of analytical grade. All solutions used in this study were prepared by dissolving the necessary reagents in deionized water.

1.2. Experimental procedure

Experiments were performed in 250 mL glass beakers at room temperature (20 ± 2°C). 200 mL of a 20 mg/L PNP solution was added into the reaction vessel. A certain amount of the STPP

ligand (25, 50, 75, and 100 mmol/L) was dissolved in the PNP solution and 1 mol/L NaOH and H_2SO_4 solutions were utilized to adjust the solutions to the desired pH value (3.0, 5.0, 7.0, 8.0 and 9.0). The reaction mixture was then bubbled with air at a flow rate of 150 mL/min. The experimental solution was mixed by a magnetic stirrer throughout the whole process. The reaction was initiated by dosing ZVC into the solution at a concentration of 0.8 g/L unless otherwise specified. Samples (1 mL) were taken from the reactor at predetermined times and quenched upon the addition of a small amount of ethanol (0.1 mol/L). The concentration of PNP was measured immediately using high performance liquid chromatography (HPLC) (Agilent 1100, USA). All experiments were run in duplicates or triplicates. Values shown are means of multiple independent samples with error bars corresponding to the standard deviation. The relative errors were less than ±5%.

To identify the ROS generated during the reaction, 3-CCA (coumarin-3-carboxylic acid) and NBT (nitroblue tetrazolium chloride) were used as probe compounds for ·OH and $O_2{\cdot}^-$, respectively, and their post-reaction products (7-OHCCA and deep-blue diformazan form, respectively) were analyzed. In addition, an excess amount of TBA (·OH scavenger) and catalase (H_2O_2 scavenger) were used in the experiment to evaluate the contribution from different ROS to the PNP degradation process.

1.3. Characterization

The structure and morphology of the samples were characterized by X-ray powder diffraction (XRD, Ultima IV, Japan) and transmission electron microscopy (TEM, JEM-2100F, Japan). X-ray photoelectron spectroscopy (XPS) was performed on a ESCALAB 250 X-ray photoelectron spectrometer (Thermo, USA). Curve calculations were achieved using the XPS Peak 4.1 program.

1.4. Analytical method

The concentration of PNP was analyzed by HPLC (1100, Agilent, America) with an Agilent TC-C18 column (150 mm × 4.6 mm, 5 μm) (Subbulekshmi and Subramanian, 2017). The maximum absorption wavelength of PNP was determined and selected as 317 nm. The eluent consisted of 50/50 (V/V) of acetonitrile/0.1% formic acid at a flow rate of 1.0 mL/min. The injective volume was 10 μL. Gas chromatography/mass spectrometry (GC/MS, 6890/5973, Agilent, USA) and liquid chromatography-mass spectrometry (LC-MS, TSQ, Thermo, USA) were used to identify of the intermediate products formed during the PNP degradation process. For GC/MS, samples (200 mL) were collected at different reaction times (10, 20, 40 and 60 min). First, the samples were extracted three times with ethyl acetate and then dried using anhydrous sodium sulfate. The samples were then concentrated in vacuo at 65°C. After the pretreatment step, 1 μL of the sample was injected in splitless mode. The oven temperature was initiated at 40°C and held for 3 min, and then increased to 200°C at 20°C/min and held for 5 min, after that the temperature was increased to 250°C at 10°C/min and held for 5 min. The flow rate of the carrier gas helium was 1.0 mL/min. Mass spectra were obtained in EI mode with an electron energy of 70 eV. For LC/MS, 20 μL of the extract dissolved in acetonitrile was automatically injected into the LC-MS system. The eluent was the same as that used for HPLC and the flow rate was 0.2 mL/min. The MS spectra were acquired over a *m/z* range of 40–200 in negative scan mode.

The 2,9-dimethyl-1,10-phenant-hroline (DMP) method was used to determine the concentration of Cu^+ (Tran et al., 1998). After the sample was taken at the predetermined time, 1 mL DMP (1 g/L) was added and water was added to make the final volume of 5 mL. The Cu^+-DMP complex was measured on a UV spectrophotometer at 460 nm. When the total copper ion (TCu) was measured, ascorbic acid was utilized as the reductant.

The concentration of H_2O_2 was determined by KI iodine blue spectrophotometry (Zhang, 2010). The redox reaction of KI and H_2O_2 under acidic conditions produces iodine. Iodine reacts with starch to produce a blue complex with an intense absorption maximum at 585 nm.

$O_2{\cdot}^-$ and ·OH were detected by electron paramagnetic resonance (EPR) spectroscopy. 5,5-dimethyl-1-pyrroline N-oxide (DMPO) was used as the spin trap agent.

2. Results and discussion

2.1. PNP degradation in the different reaction systems studied

In this study, STPP, EDTA and sodium oxalate were chosen as representative ligands to evaluate their contribution to the degradation of PNP in the ZVC/O_2 system under neutral conditions. As shown in Fig. 1a, PNP was completely degraded in the ZVC/O_2/STPP system within 120 min, while its degradation was <10% in the presence of EDTA or sodium oxalate. These results showed that STPP was a superior ligand to the other studied in the ZVC/O_2 system. The control experiments displayed in Fig. 1b shows that ZVC, ZVC/O_2 or ZVC/STPP/N_2 hardly degrade PNP, which indicated that PNP removal via volatilization and adsorption by ZVC was negligible. The TOC was reduced by 42.8% after 120 min of reaction in the ZVC/O_2/STPP system, which confirmed that a substantial quantity of PNP was mineralized. Appendix A Fig. S1 shows the variation in the concentration of dissolved oxygen (DO) in the ZVC/O_2/STPP system. It was observed that the concentration of DO decreased once the reaction began, further indicating that DO was rapidly activated in the presence of STPP. Based on the above results, it was inferred that PNP was oxidatively degraded by the ZVC/O_2/STPP system.

2.2. Effective copper species used to activate O_2

It has been reported in the literature that the low reducibility of ZVC prevents it from effectively reducing O_2 into ROS (Harford and Sarkar, 1997). Therefore, Cu^+ is considered to be the main substance to activate O_2 in the system. In order to verify the role of Cu^+ in the PNP degradation process in the ZVC/O_2/STPP system, we investigated the degradation of PNP employing DMP as a chelating agent for Cu^+. As shown in Fig. 2a, only 3.8% PNP was removed after 120 min in the presence of an excess amount of DMP. This small amount of

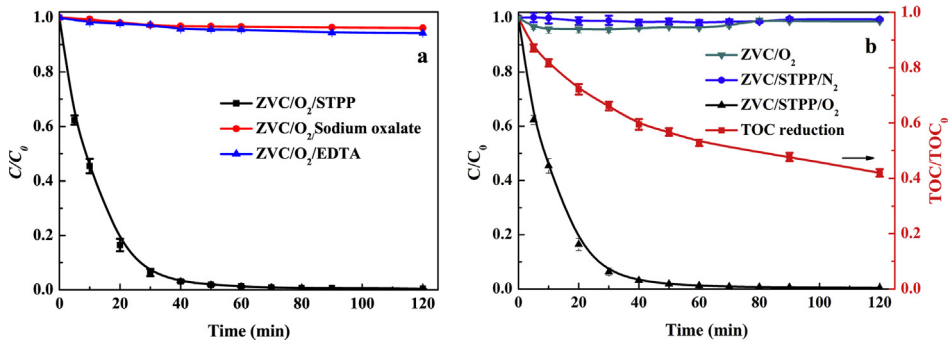

Fig. 1 – (a) The effect of various ligands on the degradation of PNP in the ZVC/O_2 system under neutral conditions. (b) PNP degradation in the ZVC/O_2/STPP system using different control experiments and the evolution of TOC as a function of the reaction time. Experimental conditions: ZVC = 0.8 g/L, PNP = 20 mg/L, initial pH = 7.0, STPP = 6.25 mmol/L.

PNP degradation was because Cu^0 activates O_2 to produce ·OH (Eqs. (5) and (6)). However, because the contribution of this reaction pathway to PNP degradation is negligible, it was not discussed in depth in this study. We monitored the release of Cu^+ and Cu^{2+} in the system during the reaction (Appendix A Fig. S2). The concentration of TCu increased gradually and reached up to 400 mg/L at 60 min. However, the concentration of Cu^+ was maintained at a low level during the reaction because Cu^+ is quickly oxidized to Cu^{2+}, so the Cu^{2+} measured in the system constituted >97.5% of total copper ions released. The release of Cu^+ was attributed to the corrosion of ZVC by O_2 in the presence of STPP. We used Cu^+ (using a CuCl precursor) with the same molar amount as the TCu released in the system to degrade PNP. The results in Fig. 2b show that the degradation curves of PNP in the two systems were almost identical. These results clearly suggested that the Cu^+ species in the system were the main reducing agent for the activation of O_2 to produce ROS. The main role of ZVC in the system was as a continuous dissolution source of Cu^+. This conclusion is consistent with the results reported previously (Ma et al., 2018; Zhang et al., 2017).

$$Cu + O_2 + H_2O \rightarrow Cu^{2+} + H_2O_2 + 2OH^- \quad (5)$$

$$Cu + H_2O_2 + H^+ \rightarrow Cu^{2+} + \cdot OH + H_2O \quad (6)$$

The surface morphology and elemental composition of the fresh and reacted ZVC particles used in the ZVC/O_2/STPP system were characterized using XRD, TEM and XPS. The XRD results in Fig. 3c show that the diffraction peaks matched well with the standard pattern of ZVC (JCPDS-PDF: 04-0836). No other peaks were detected, suggesting the fresh copper powder was mainly made up of Cu^0 and no oxide film was formed on the surface. The TEM images showed that the spherical particles of the copper powder had diameters of ~100 nm and a very smooth surface (Fig. 3a). After the reaction, the diffraction peaks at 29.554 and 61.334° for cuprous oxide (JCPDS-PDF:04-0836) suggested that Cu^+ was generated during the reaction. The TEM images showed that obvious surface defects and holes were present on the used ZVC particles, indicating that the ZVC was seriously corroded (Fig. 3b). When combined with the high resolution XPS spectra of Cu 2p shown in Fig. 3d, some Cu^+ and Cu^{2+} ions were formed on the surface of ZVC during the reaction. According to the above characterization results, some copper (hydrogen) oxide may be formed on the surface of the ZVC particles during the reaction, which inhibited the further corrosion of ZVC. In addition, the EDS spectrum of ZVC after the reaction in the presence or absence of STPP is shown in Appendix A Fig. S3. It can be found that the oxygen element content on the surface of ZVC particles reacted with STPP is about 2.7 times that

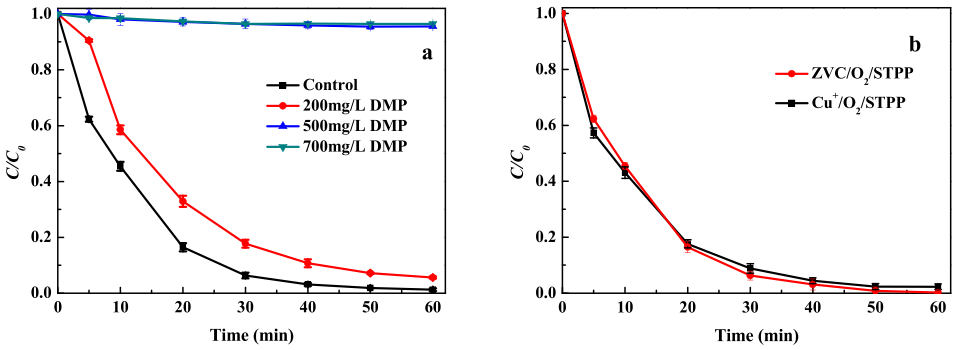

Fig. 2 – (a) The effect of the addition of DMP (Cu^+ scavenger) on the degradation of PNP in the ZVC/O_2/STPP system. (b) The PNP degradation curves obtained for the ZVC/O_2/STPP and Cu^+/O_2/STPP systems using the same copper ion concentration. Experimental conditions: ZVC = 0.8 g/L, PNP = 20 mg/L, initial pH = 7.0, STPP = 6.25 mmol/L, Cu^+ = 0.4 g/L.

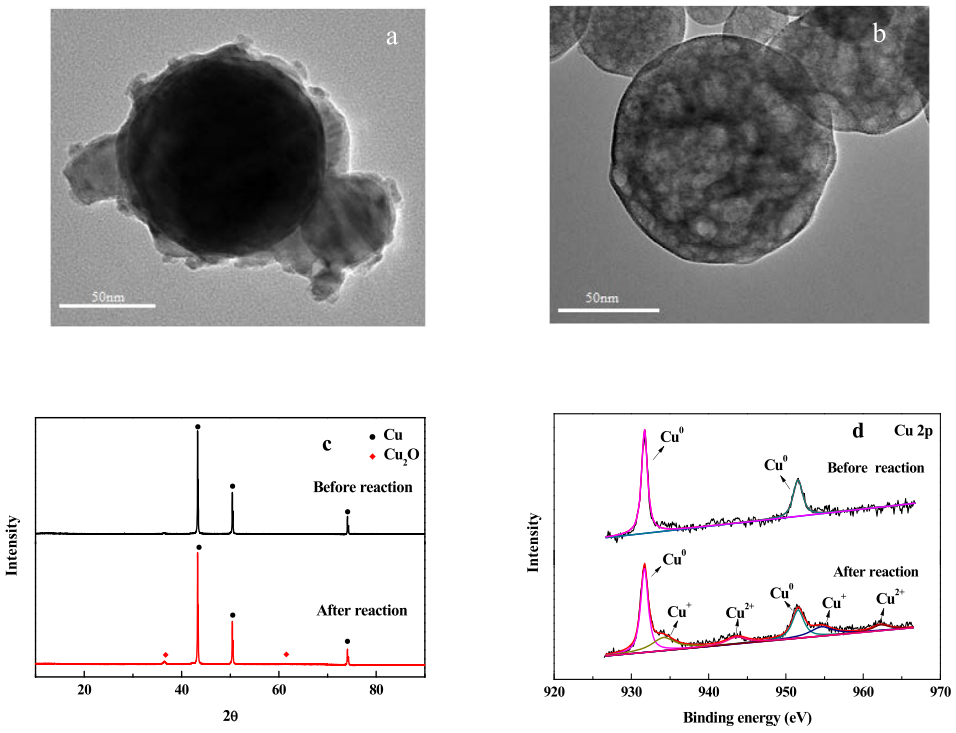

Fig. 3 – TEM images of the (a) fresh and (b) reacted ZVC particles used in the ZVC/O_2/STPP system. (c) XRD patterns of the ZVC powder before and after the PNP degradation reaction. (d) The high resolution XPS spectra of Cu 2p in ZVC before and after the PNP degradation experiment.

without STPP. This result strongly proves that STPP accelerates the corrosion of ZVC in the system.

2.3. *Degradation mechanism of PNP using the ZVC/O_2/STPP system*

2.3.1. *Reactive radical generation*

According to previous studies, the ROS produced by Cu^+ activation of O_2 in solution included H_2O_2, $O_2{\cdot}^-$ and ·OH. To confirm the type of ROS produced in the ZVC/O_2/STPP system, we utilized EPR spectroscopy with DMPO spin-trapping adducts to perform the analysis and the results are shown in Fig. 4a. Only the characteristic peaks of ·OH were detected in the ZVC/O_2/STPP system, and the other ROS characteristic peaks (such as $O_2{\cdot}^-$ and $^1O_2$) were not found, indicating that STPP can effectively promote the production of ·OH in the system (Fadda et al., 2017; Zhu et al., 2018). To further validate the results of the EPR analysis, we designed two groups of probe experiments. The experiments were carried out using NBT as a probe for $O_2{\cdot}^-$ (Sirota, 2017) and 3-CCA as a probe for ·OH (Baldacchino et al., 2009) and the reaction specific products were detected using spectrophotometry and the results are shown in Fig. 4b. The amount of ·OH increased continuously after the experiment began. Meanwhile, $O_2{\cdot}^-$ was still not detected in the system. Combining the results of the above two experiments, we found that in the ZVC/O_2/STPP system, ·OH was generated via the double-electron activation of oxygen ($O_2 \rightarrow H_2O_2 \rightarrow$ ·OH). We could detect the presence of H_2O_2 using KI iodine blue spectrophotometry. As shown in Fig. 4c, the amount of H_2O_2 increased almost linearly, confirming that Cu^+ could reduce O_2 to H_2O_2. Subsequently, we studied the roles of H_2O_2 and ·OH in the degradation of PNP. We added catalase (a H_2O_2 scavenger, 500 mg/L) and TBA (a ·OH scavenger, 20 mmol/L) as scavengers into the ZVC/O_2/STPP solution. As shown in Fig. 4d, TBA and catalase completely inhibited the degradation of PNP. Considering the fact that H_2O_2 alone did not degrade PNP (Appendix A Fig. S4), this result suggests that ·OH was solely responsible for the degradation of PNP in the ZVC/O_2/STPP system. H_2O_2 was an important intermediate serving as the ·OH precursor.

2.3.2. *Possible degradation pathway of PNP*

PNP can be removed efficiently in the system. However, it can be observed from Fig. 1b that the TOC removal of PNP was much slower than its decomposition, indicating that some of the intermediates derived from PNP decomposition remained in solution. GC-MS analysis was employed to further identify the intermediate products formed at different reaction times (10, 20, 40 and 60 min) and the mass spectra displayed in Appendix A Fig. S5 and Table S1. The main intermediates observed during the first 20 min of the reaction were p-benzoquinone, hydroquinone, p-nitrocatechol and PNP. After the reaction was carried out for 40 min, the aromatic ring was cleaved, and some esters and alcohols, such as 3-oxobuty acetate, ethyl butyrate and butyl acetate, were generated. The LC-MS results shows that small acids such as formic acid and acetic acid were detected in the system. The reaction pathway for the degradation of PNP is proposed in Fig. 5. In this pathway, the nitro group located in the para-position on the aromatic ring was substituted by ·OH to yield hydroquinone. Meanwhile, the electrophilic ·OH group could be added onto the aromatic ring of PNP, resulting in the formation of p-

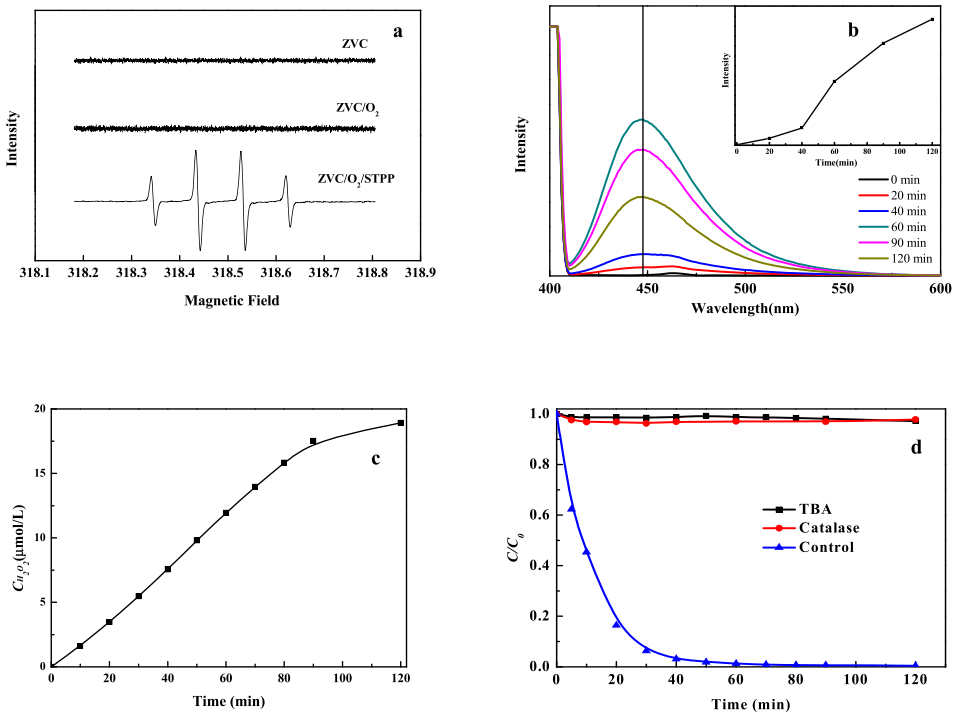

Fig. 4 – (a) DMPO spin-trapping EPR spectra recorded for ·OH in different reaction system. (b) The fluorescence spectra of 3-CCA for ·OH detection in the system. (c) The detection of H_2O_2 generated in the system using spectrophotometry at 585 nm. (d) PNP degradation in the presence of TBA as a ·OH scavenger and catalase as a H_2O_2 scavenger. Experimental conditions: ZVC = 0.8 g/L, PNP = 20 mg/L, initial pH = 7.0, STPP = 6.25 mmol/L.

nitrocatechol. Further oxidation of the hydroquinone and p-nitrocatechol yielded esters, which were degraded into smaller molecular organic acids and further mineralized into CO_2 and H_2O. From the above experimental results, it can be seen that p-aminophenol (the reaction product of $O_2\cdot^-$and PNP) was not detected in the system, which further proved that the ROS production pathway in the ZVC/O_2/STPP system was $O_2 \rightarrow H_2O_2 \rightarrow$ ·OH. ·OH plays a crucial role in the degradation of PNP.

2.4. *The roles of STPP in the system*

The use of chelating agents to promote the corrosion of metals in aqueous solutions is important in corrosion science and corrosion protection engineering. In order to prove that STPP can effectively promote ZVC corrosion by O_2 under neutral conditions, we determined the release of TCu in the reaction system. As shown in Fig. 6a, the release of TCu from the ZVC/O_2/STPP system was up to 400 mg/L, accounting for 50% of the ZVC in the system, while the release of TCu in the ZVC/O_2 system was almost negligible. Appendix A Fig. S6 shows that the degradation rate of PNP in the system was linear with the concentration of TCu ($R^2 = 0.99$). The above experimental results showed that STPP promoted the release of Cu^{2+}/Cu^{+} from ZVC under neutral conditions through its complexation, thereby improving the degradation of PNP in the system. The redox abilities of Cu^{+} and Cu^{+}-STPP were investigated with the aid of cyclic voltammograms (CV) measurement. The

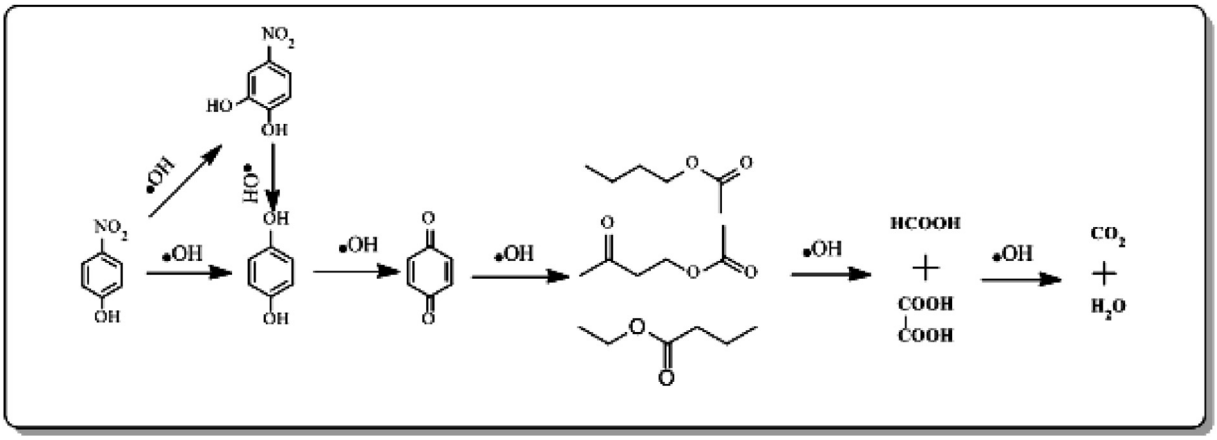

Fig. 5 – A possible pathway for PNP degradation in the ZVC/O_2/STPP system.

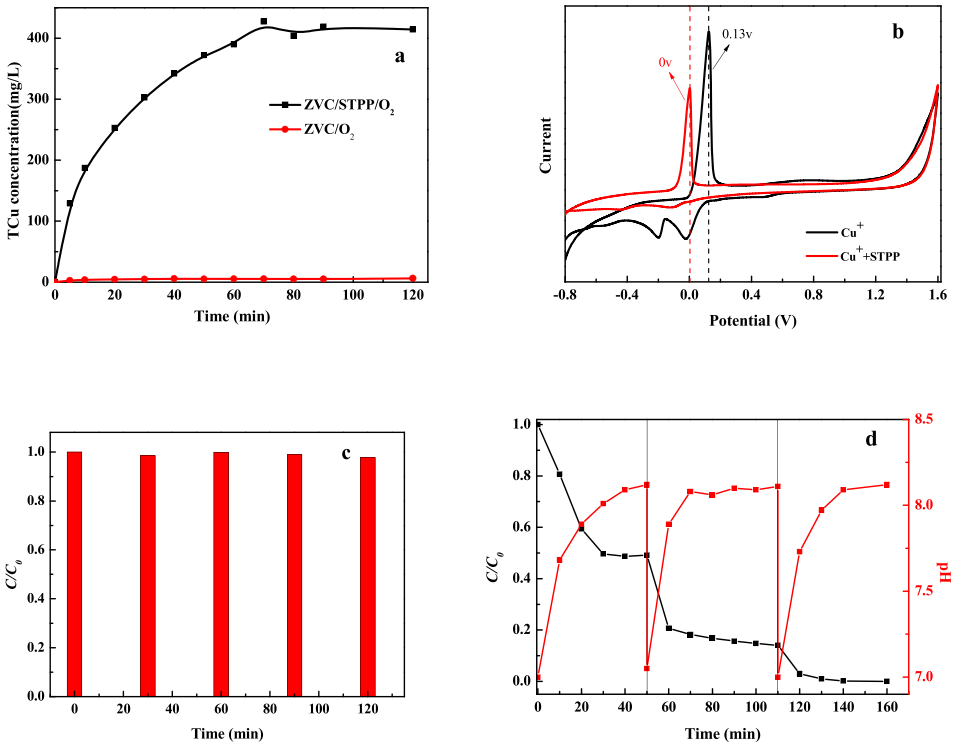

Fig. 6 – (a) The TCu concentration generated in the ZVC/O_2 and ZVC/O_2/STPP systems. (b) Cyclic voltammograms recorded for Cu^+ and Cu^+-STPP solutions. (c) The variation in the STPP concentration during the reaction. (d) The degradation curve of PNP after re-adjusting the solution to pH = 7. Experimental conditions: ZVC = 0.8 g/L, PNP = 80 mg/L, initial pH = 7.0, STPP = 6.25 mmol/L.

results are shown in Fig. 6b. The electrodes were cycled from −0.8 to +1.6 V at a scan rate of 10 mV/sec. For the Cu + solution, the oxidation peak formed from Cu^+ oxidation to Cu^{2+} was observed at 0.13 V during positive scan. After the STPP ligand was added, the positive peak potential dropped to 0 V. This demonstrated that the addition of STPP makes Cu^+ more easily oxidized to Cu^{2+}, effectively decreased the redox potential of Cu^{2+}/Cu^+, promoting Cu^+ to activate O_2 to produce ·OH. In summary, there are two main functions of STPP in the system. On the one hand, STPP accelerated the corrosion of ZVC and promote the release of Cu^+. On the other hand, it promoted the generation of ·OH in the system. We then determined the STPP content in the system before and after the reaction using ion chromatography. As shown in Fig. 6c, the results showed that STPP maintained its initial concentration throughout the reaction. Under the conditions of sufficient ZVC and O_2, what is the reason for the termination of the reaction. We speculated that pH was the main controlling factor. To confirm our hypothesis, the solution was readjusted to pH = 7 after termination of the reaction in the ZVC/O_2/STPP system and the concentration of PNP and pH in the system was determined. As shown in Fig. 6d, the PNP in the system could still be effectively degraded after re-adjusting the pH of the solution. In addition, it could be seen from the pH curve, when the solution pH reached 8.1, the degradation of PNP in the system stopped. This indicated that when the solution pH was >8.1, the complexation of STPP was not enough to enhance the further corrosion of ZVC by O_2. At pH < 8.1, STPP was recycled to continuously promote ZVC corrosion. Therefore, the reaction was initiated and terminated by adjusting the pH of the system.

2.5. *The effects of different factors on the PNP degradation process*

Based on the above experimental results, the solution pH was a crucial factor in the PNP degradation process. We studied the effect of the initial pH on the degradation of PNP by adding

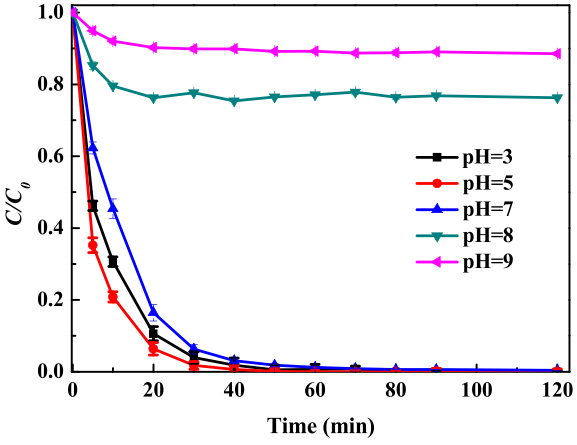

Fig. 7 – The PNP degradation curves obtained at different initial pH values. Experimental conditions: ZVC = 0.8 g/L, PNP = 20 mg/L, STPP = 6.25 mmol/L.

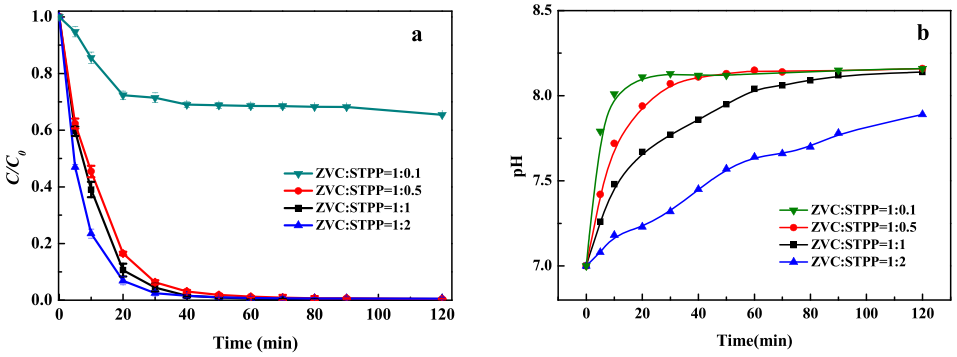

Fig. 8 – The PNP degradation curve (a) and solution pH (b) versus time obtained at different molar ratios of ZVC/STPP. Experimental conditions: ZVC = 0.8 g/L, PNP = 20 mg/L, initial pH = 7.0.

different amounts of HCl/NaOH. As shown in Fig. 7, PNP was rapidly removed in the ZVC/O_2/STPP system at initial pH values of 3.0, 5.0 and 7.0. At an initial pH value of 8.0, the system exhibited only a slight degradation capacity with only 23.7% of the PNP being removed from the solution. This was attributed to the rapid rise of the solution pH to 8.1. Therefore, lower pH was favorable for the corrosion of ZVC (Li et al., 2013). However, the STPP ligand may be protonated at a sufficiently low pH value, which reduces its ability to promote O_2 activation by Cu^+, thereby inhibiting the PNP degradation process. Therefore, under the combined effect of these two factors, the optimal pH of the reaction system was 5.0. In addition, we found that 10% of PNP was still degraded when the initial pH of the solution was 9.0. The reason for this phenomenon was due to the release of only a small amount of Cu^+ on the surface of ZVC under the effect of STPP at the beginning of the reaction. Then, the ZVC was passivated and the reaction was terminated.

Besides the pH value, PNP degradation in the ZVC/O_2/STPP system also depends on the STPP dosage. We kept the amount of ZVC in this system unchanged and set the ZVC/STPP molar ratio to 1:0.1, 1:0.5, 1:1 and 1:2, respectively. The degradation performance is shown in Fig. 8a, the degradation efficiency of PNP increased upon increasing the STPP concentration. The role of STPP has been described in detail in Section 2.4 of this paper. In addition, as shown in Fig. 8b, STPP had a buffering effect and the reaction time became longer upon increasing the STPP concentration, which was also beneficial for the degradation of PNP. At ZVC/STPP = 1:0.1, the degradation of PNP was terminated when the pH increased to around 8.1, which was the same as that observed in the abovementioned experimental results.

Previous research studies have shown that ZVC nanoparticles tend to have higher reactivity than their corresponding microparticles (Liou et al., 2007; Li et al., 2014). In order to study the effect of the ZVC particle size on the degradation of PNP, four particle sizes (100 nm, 5 μm, 10 μm and 44 μm) were selected for our experiments. As shown in Fig. 9a, PNP was completely degraded in the different systems, indicating that the O_2 activation reaction can continuously occur in the ZVC/O_2/STPP system in the presence of a sufficient copper source. It can be seen from Fig. 9b that the PNP degradation process obeyed first-order kinetics. Among them, the micron-scale ZVC/O_2/STPP system displayed two-stage first-order kinetics. The first-stage was mostly ascribed to the relatively small surface area of the micron-scale ZVC, which caused its low reactivity. The rapid degradation stage (second-stage) was attributed to the corrosion of the ZVC surface to form a large number of defects and holes, increasing the specific surface area of the reaction. In general, the degradation rate of PNP increased upon decreasing the ZVC particle size. This was because ZVC with a smaller particle size had a larger specific surface area and higher surface reactivity.

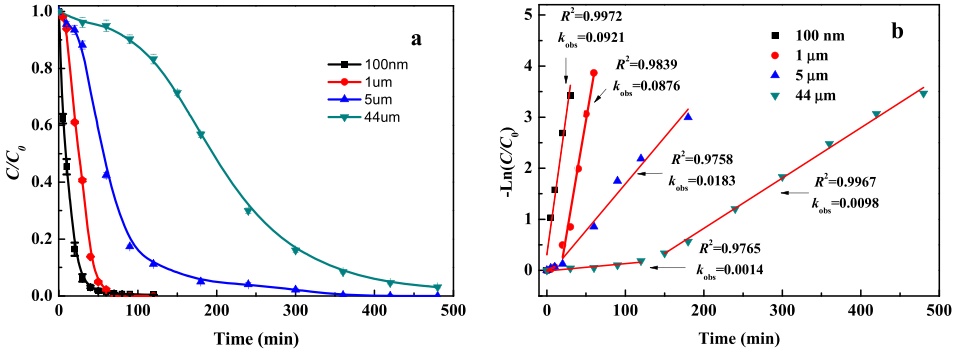

Fig. 9 – The PNP degradation curve (a) and plot of -ln(C/C_0) (b) versus time obtained using different ZVC particle sizes. Experimental conditions: ZVC = 12.5 mmol/L, PNP = 20 mg/L, initial pH = 7.0, STPP = 6.25 mmol/L.

3. Conclusions and environmental implications

In this study, 20 mg/L PNP was effectively degraded in the ZVC/O_2/STPP system under neutral conditions. ·OH was identified as the main ROS during the degradation of PNP in this system and its main production pathway was the double-electron activation of O_2 ($O_2 \rightarrow H_2O_2 \rightarrow$ ·OH). STPP played a crucial role in the degradation process. On one hand, when the solution pH was <8.1, the complexation of STPP promoted the corrosion of ZVC by O_2 to release Cu^+. On the other hand, STPP promoted the production of ·OH by reducing the redox potential of Cu^{2+}/Cu^+. In addition, as a food additive, STPP is relatively safe and cheap for environmental applications. The experimental results showed that STPP was reused in the system. At pH < 8.1, the system continuously degraded organic pollutants. Therefore, we can initiate and terminate the reaction by controlling the pH of the system. In addition, the contamination of released copper ions can be controlled by adjusting the pH of the solution. As shown in Appendix A Fig. S7, When the pH value of the solution was increased to 12, a large amount of Cu^{2+} was precipitated, thereby reducing its concentration to 1 mg/L (the Discharge Standard of Pollutants for Municipal Wastewater Treatment Plant of China (GB 18918-2002)). This is easily achieved in industrial wastewater treatment.

Acknowledgments

This work was financially supported by the Fundamental Research Funds for the Central Universities of China, and Key Project of National Natural Science Foundation of China (No. 41530636).

Appendix A. Supplementary data

Supplementary data to this article can be found online at https://doi.org/10.1016/j.jes.2020.01.001.

REFERENCES

Baldacchino, G., Maeyama, T., Yamashita, S., Taguchi, M., Kimura, A., Katsumura, Y., et al., 2009. Determination of the time-dependent OH-yield by using a fluorescent probe. Application to heavy ion irradiation. Chem. Phys. Lett. 468, 275–279.

Bokare, A.D., Wonyong, C., 2009. Zero-valent aluminum for oxidative degradation of aqueous organic pollutants. Environ. Sci. Technol. 43, 7130–7135.

Cinar, S.A., Ziylan-Yavaş, A., Catak, S., Ince, N.H., Aviyente, V., 2017. Hydroxyl radical-mediated degradation of diclofenac revisited: a computational approach to assessment of reaction mechanisms and by-products. Environ. Sci. Pollut. Res. 24, 18458–18469.

Deng, J., Xu, M., Chen, Y., Li, J., Qiu, C., Li, X., et al., 2019. Highly-efficient removal of norfloxacin with nanoscale zero-valent copper activated persulfate at mild temperature. Chem. Eng. J. 366, 491–503.

Dong, G., Ai, Z., Zhang, L., 2014. Total aerobic destruction of azo contaminants with nanoscale zero-valent copper at neutral pH: Promotion effect of in-situ generated carbon center radicals. Water Res 66, 22–30.

Fadda, A., Barberis, A., Sanna, D., 2017. Influence of pH, buffers and the role of quinolinic acid, a novel iron chelating agent, in the determination of hydroxyl radical scavenging activity of plant extracts by Electron Paramagnetic Resonance (EPR). Food Chem 240, 174.

Feng, Y., Lee, P.H., Wu, D., Zhou, Z., Li, H., Shih, K., 2017. Degradation of contaminants by Cu^+-activated molecular oxygen in aqueous solutions: Evidence for cupryl species (Cu^{3+}). J. Hazard. Mater. 331, 81–87.

Harford, C., Sarkar, B., 1997. Amino terminal Cu(II)- and Ni(II)-binding (ATCUN) motif of proteins and peptides: Metal binding, DNA cleavage, and other properties. ChemInform 28, 123–130.

Huang, C.C., Lo, S.L., Lien, H.L., 2012. Zero-valent copper nanoparticles for effective dechlorination of dichloromethane using sodium borohydride as a reductant. Chem. Eng. J. 203, 95–100.

Joseph, C.G., Gianluca, L.P., Awang, B., Duduku, K., 2009. Sonophotocatalysis in advanced oxidation process: a short review. Ultrason. Sonochem. 16, 583–589.

Keenan, C.R., Sedlak, D.L., 2008. Factors affecting the yield of oxidants from the reaction of nanoparticulate zero-valent iron and oxygen. Environ. Sci. Technol. 42, 1262–1267.

Lee, H., Lee, H.J., Seo, J., Kim, H.E., Shin, Y.K., Kim, J.H., et al., 2016. Activation of oxygen and hydrogen peroxide by copper(II) coupled with hydroxylamine for oxidation of organic contaminants. Environ. Sci. Technol. 50, 8231.

Lee, C., Yoon, J., Gunten, U.V., 2007. Oxidative degradation of N-nitrosodimethylamine by conventional ozonation and the advanced oxidation process ozone/hydrogen peroxide. Water Res 41, 581–590.

Li, H., Wan, J., Ma, Y., Yan, W., Huang, M., 2014. Influence of particle size of zero-valent iron and dissolved silica on the reactivity of activated persulfate for degradation of acid orange 7. Chem. Eng. J. 237, 487–496.

Li, W., Feng, W., Li, P., Zhang, L., 2013. Ferrous–tetrapolyphosphate complex induced dioxygen activation for toxic organic pollutants degradation. Sep. Purif. Technol. 120, 148–155.

Lin, C.J., Lo, S.L., Liou, Y.H., 2005. Degradation of aqueous carbon tetrachloride by nanoscale zerovalent copper on a cation resin. Chemosphere 59, 1299–1307.

Lin, K., Cai, J., Sun, J., Xue, X., 2014. Removal of 2,4-dichlorophenol by aluminium/O_2/acid system. J. Chem. Technol. Biotechnol. 88, 2181–2187.

Liou, Y.H., Shang, L.L., Lin, C.J., 2007. Size effect in reactivity of copper nanoparticles to carbon tetrachloride degradation. Water Res 41, 1705–1712.

Liu, W., Zhang, H., Cao, B., Lin, K., Gan, J., 2011. Oxidative removal of bisphenol A using zero valent aluminum–acid system. Water Res 45, 1872–1878.

Ma, X., Cheng, Y., Ge, Y., Wu, H., Li, Q., Gao, N., et al., 2018. Ultrasound-enhanced nanosized zero-valent copper activation of hydrogen peroxide for the degradation of norfloxacin. Ultrason. Sonochem. 40, 763–772.

Matzek, L.W., Carter, K.E., 2016. Activated persulfate for organic chemical degradation: A review. Chemosphere 151, 178–188.

Michael, S., Anke, P., Martin, J., 2011. Treatment of pharmaceuticals and diagnostic agents using zero-valent iron–kinetic studies and assessment of transformation products assay. Environ. Sci. Technol. 45, 4944–4950.

Moffett, J.W., Zika, R.G., 1987. Reaction kinetics of hydrogen peroxide with copper and iron in seawater. Environ. Sci. Technol. 21, 804–810.
Noradoun, C.E., I Francis, C., 2005. EDTA degradation induced by oxygen activation in a zerovalent iron/air/water system. Environ. Sci. Technol. 39, 7158–7163.
Saritha, P., Aparna, C., Himabindu, V., Anjaneyulu, Y., 2007. Comparison of various advanced oxidation processes for the degradation of 4-chloro-2 nitrophenol. J. Hazard. Mater. 149, 609–614.
Sirota, T.V., 2017. Standardization and regulation of the rate of the superoxide-generating reaction of adrenaline autoxidation used for evaluation of pro/antioxidant properties of various materials. Biochemistry (Moscow) 11, 128–133.
Subbulekshmi, N.L., Subramanian, E., 2017. Nano CuO immobilized fly ash zeolite Fenton-like catalyst for oxidative degradation of p-Nitrophenol and p-Nitroaniline. J. Environ. Chem. Eng. 5, 1360–1371.
Tamura, H., Ito, N., Kitano, M., Takasaki, S., 2001. A kinetic model of the dissolution of copper(II) oxide in EDTA solutions considering the coupling of metal and oxide ion transfer. Corros. Sci. 43, 1675–1691.
Tran, D., Skelton, B.W., White, A.H., Laverman, L.E., Ford, P.C., 1998. Investigation of the nitric oxide reduction of the Bis (2, 9-Dimethyl-1, 10-phenanthroline) complex of copper (II) and the structure of [Cu (dmp) $_2$ (H_2O)](CF_3SO_3) $_2$. Inorg. Chem. 37, 2505–2511.
Welch, K.D., Davis, T.Z., Aust, S.D., 2002. Iron autoxidation and free radical generation: effects of buffers, ligands, and chelators. Arch. Biochem. Biophys. 397, 360–369.
Xiu, Y., A Ninh, P., Guowei, X., Rose, A.L., T David, W., 2012. Effects of pH, chloride, and bicarbonate on Cu(I) oxidation kinetics at circumneutral pH. Environ. Sci. Technol. 46, 1527–1535.
Yan, Z., Gao, M.M., Wang, X.H., Wang, S.G., Liu, R.T., 2015. Enhancement of oxygen diffusion process on a rotating disk electrode for the electro-Fenton degradation of tetracycline. Electrochim. Acta 182, 73–80.
Zhang, X., 2010. Catalytic-Kinetic spectrophotometric determination of trace manganese in ores. J. Hebei Univ. 38, 125–134.
Zhang, Y., Fan, J., Yang, B., Huang, W., Ma, L., 2017. Copper-catalyzed activation of molecular oxygen for oxidative destruction of acetaminophen: The mechanism and superoxide-mediated cycling of copper species. Chemosphere 166, 89–95.
Zhao, C., Zhou, Y., Huang, W., Sun, Y., Wang, L., Zheng, H., 2014. Influence of characteristic of zeolite on loading Nano-TiO_2 for photocatalytic degradation of oxytetracyline in aqueous solution. J. Civil Archit. Environ. Eng. 36, 115–120.
Zhou, P., Zhang, J., Zhang, Y., Liu, Y., Liang, J., Liu, B., et al., 2016. Generation of hydrogen peroxide and hydroxyl radical resulting from oxygen-dependent oxidation of L-ascorbic acid via copper redox-catalyzed reactions. RSC Adv. 6, 38541–38547.
Zhou, P., Zhang, J., Zhang, Y., Zhang, G., Li, W., Wei, C., et al., 2017. Degradation of 2,4-dichlorophenol by activating persulfate and peroxomonosulfate using micron or nanoscale zero-valent copper. J. Hazard. Mater. 1209–1219.
Zhou, S., Yu, Y., Sun, J., Zhu, S., Deng, J., 2018. Oxidation of microcystin-LR by copper (II) coupled with ascorbic acid: Kinetic modeling towards generation of H_2O_2. Chem. Eng. J. 333, 443–450.
Zhu, C., Zhu, F., Liu, C., Ning, C., Gao, J., 2018. Reductive Hexachloroethane degradation by $S_2O_8^{\cdot-}$ with thermal activation of persulfate under anaerobic conditions. Environ. Sci. Technol. 52, 8548–8557.